JOURNAL OF GEOPHYSICAL RESEARCH: SPACE PHYSICS, VOL. 118, 7714–7727, doi:10.1002/2013JA018979, 2013

The detailed spatial structure of field-aligned currents comprising the substorm current wedge

Kyle R. Murphy,[1] Ian R. Mann,[1] I. Jonathan Rae,[1,6] Colin L. Waters,[2] Harald U. Frey,[3] Andy Kale,[1] Howard J. Singer,[4] Brian J. Anderson,[5] and Haje Korth[5]

Received 24 April 2013; revised 31 October 2013; accepted 1 November 2013; published 26 December 2013.

[1] We present a comprehensive two-dimensional view of the field-aligned currents (FACs) during the late growth and expansion phases for three isolated substorms utilizing in situ observations from the Active Magnetosphere and Planetary Electrodynamics Response Experiment and from ground-based magnetometer and optical instrumentation from the Canadian Array for Realtime Investigations of Magnetic Activity and Time History of Events and Macroscale Interactions during Substorms ground-based arrays. We demonstrate that the structure of FACs formed during the expansion phase and associated with the substorm current wedge is significantly more complex than a simple equivalent line current model comprising a downward FAC in the east and upward FAC in the west. This two-dimensional view demonstrates that azimuthal bands of upward and downward FACs with periodic structuring in latitude form across midnight and can span up to 8 h of magnetic local time. However, when averaged over latitude, the overall longitudinal structure of the net FACs resembles the simpler equivalent line current description of the substorm current wedge (SCW). In addition, we demonstrate that the upward FAC elements of the structured SCW are spatially very well correlated with discrete aurora during the substorm expansion phase and that discrete changes in the FAC topology are observed in the late growth phase prior to auroral substorm expansion phase onset. These observations have important implications for determining how the magnetosphere and ionosphere couple during the late growth phase and expansion phase, as well as providing important constraints on the magnetospheric generator of the FACs comprising the SCW.

Citation: Murphy, K. R., I. R. Mann, I. J. Rae, C. L. Waters, H. U. Frey, A. Kale, H. J. Singer, B. J. Anderson, and H. Korth (2013), The detailed spatial structure of field-aligned currents comprising the substorm current wedge, *J. Geophys. Res. Space Physics*, *118*, 7714–7727, doi:10.1002/2013JA018979.

1. Introduction

[2] The substorm current wedge is an integral feature of the substorm expansion phase [*McPherron et al.*, 1973]. Following auroral substorm onset [*Akasofu*, 1964], the nightside magnetotail dipolarizes [*Cummings et al.*, 1968] and the westward electrojet enhances [*Rostoker et al.*, 1975] leading to the formation of current systems in the ionosphere and magnetosphere which are known as the substorm current wedge (SCW). Typically, the SCW is viewed as an equivalent line current system consisting of a downward field-aligned current (FAC) in the east, an enhanced westward electrojet and an upward FAC in the west [*McPherron et al.*, 1973; *Clauer and McPherron*, 1974; *Yao et al.*, 2012], although significant deviations from this line current have been proposed [e.g., *Birn et al.*, 1999].

[3] Two-dimensional statistical views of the upward and downward FAC topology during substorms were originally compiled by *Iijima and Potemra* [1978] using magnetometer data from single-satellite passes of the TRIAD satellite, situated in a low-altitude 90 min polar orbit. These authors demonstrated that enhanced region 1 and region 2 current systems [*Iijima and Potemra*, 1976, 1978] contributed to the large-scale FACs associated with substorms. However, for individual events, *Iijima and Potemra* [1978] noted that small-scale current structures not observed in the statistical schematic were superimposed on the larger-scale regions 1 and 2 current systems. They also reported that during larger events (large auroral electrojet index, *AE*), a more complex pattern of FACs existed near the edge of the enhanced westward electrojet, being more structured than the typical nonsubstorm time region 1 and region 2 current systems. This more complicated current system was thought to be composed of an upward

[1]Department of Physics, University of Alberta, Edmonton, Alberta, Canada.
[2]School of Mathematical and Physical Sciences, University of Newcastle, Callaghan, New South Wales, Australia.
[3]Space Sciences Laboratory, University of California, Berkeley, California, USA.
[4]Space Environment Center, NOAA, Boulder, Colorado, USA.
[5]Applied Physics Laboratory, Johns Hopkins University, Laurel, Maryland, USA.
[6]Mullard Space Science Laboratory, University College London, Dorking, UK.

Corresponding author: K.R. Murphy, Department of Physics, University of Alberta, Edmonton, AB T6G 2G7, Canada. (kmurphy@ualberta.ca)

2169-9380/13/10.1002/2013JA018979

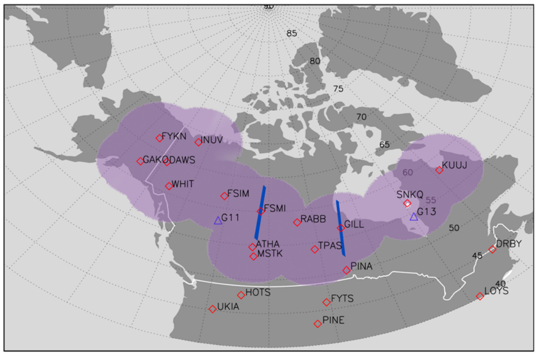

Figure 1. The location of ground-based magnetometers (diamonds); ASI and MSP fields of view (purple and blue, respectively). The north magnetic footprints of G11 and G13 are marked by blue triangles.

FAC surrounded by downward FACs to the north and south. A similar FAC topology was also observed by *Rostoker et al.* [1975] utilizing the TRIAD satellite magnetometer.

[4] In general, statistical studies of FACs compiled from single satellite can only develop an *average* picture of the large scale and predominant FACs which couple the ionosphere and magnetosphere. By their very nature, statistical studies smooth over fine-scale structures in the FAC topology. This smoothing out of the fine structure of FACs is important when considering the spatial and temporal variability of these currents through the substorm growth and expansion phase. More importantly, the assumption needed to infer FACs from single-satellite measurements is often invalid [*Peria et al.*, 2000] leading to erroneous results, both in terms of the inferred FAC magnitude but more importantly, FAC direction [*Zheng et al.*, 2003]. Specifically, single-spacecraft magnetometer measurements are subject to a space-time ambiguity which introduces an uncertainty into any derived FAC which can only be avoided utilizing multispacecraft measurements [*Peria et al.*, 2000].

[5] In this paper we use detailed multispacecraft estimates of FACs from the Iridium constellation of satellites and the Active Magnetosphere and Planetary Electrodynamics Response Experiment (AMPERE) [*Anderson et al.*, 2000; *Waters et al.*, 2001] to develop a comprehensive two-dimensional view of the FACs preceding substorm onset and the structure of the FACs comprising the SCW during the expansion phase. To date, the multispacecraft Iridium constellation and AMPERE provide the most comprehensive view of the FAC systems comprising the SCW. In this paper we exploit this in order to establish both the two-dimensional topology and the temporal evolution of these FACs through substorm onset. Such structure was previously unknown as this fine-scale structure was not detectable using single-satellite measurements. Further, we supplement the AMPERE FACs with auroral observations provided by the Time History of Events and Macroscale Interactions during Substorms (THEMIS) all-sky imagers (ASIs) [*Mende et al.*, 2008] and ground-based magnetic field observations from the Canadian Array for Realtime Investigations of Magnetic Activity (CARISMA) [*Mann et al.*, 2008] and THEMIS magnetometer arrays [*Russell et al.*, 2008]. Using these combined data sets, we demonstrate that the FACs associated with the SCW are highly structured and filamented with discrete regions of both upward and downward FACs spanning up to 8 h of magnetic local time (MLT) on the nightside. When spatially averaged (as a function of MLT), these discrete regions of upward and downward FACs resemble the equivalent line current system of the SCW described for example by *McPherron et al.* [1973]. Finally, using the AMPERE data, we are able to confirm that regions of upward FAC are typically associated with discrete auroral forms.

2. Instrumentation

[6] Multipoint observations of the magnetic field are required in order to separate the spatial variations from the temporal fluctuations of the current systems coupling the ionosphere and magnetosphere. Specifically, a multispacecraft study is capable of identifying quasi-stationary time periods during which temporal changes in the magnetic field can be neglected. When estimating FAC densities, this enables the validation of the assumption that variations in the magnetic field along a spacecraft trajectory can be interpreted as spatial variations and hence be used as an estimate for the curl of the magnetic field for determining FAC structure.

[7] AMPERE utilizes over 70 spacecraft as part of the Iridium constellation to infer the global structure of FACs from vector measurements of the magnetic field at a 20 s cadence [*Anderson et al.*, 2000; *Waters et al.*, 2001]. The Iridium satellites are distributed in six circular orbital planes at an altitude of ~780 km and a nominal separation of 4 h of local time. Utilizing the entire Iridium constellation of satellites AMPERE is able to determine the FAC topology in both the Southern and Northern Hemispheres in 10 min intervals,

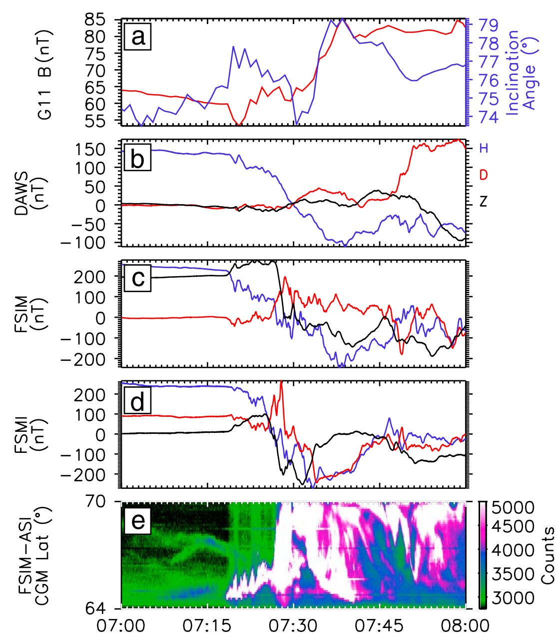

Figure 2. Summary of geosynchronous and ground-based observations for the 16 February 2010 substorm. (a) G11 total magnetic field (red) and inclination angle (blue). (b–d) *H* (blue), *D* (red), and *Z* (black) magnetic field variations from the DAWS, FSIM, and FSMI ground-based magnetometers, respectively. (e) FSIM keogram from the THEMIS ASI; the keogram is constructed from a slice through the ASI perpendicular to the growth phase arc and in the MLT sector of auroral onset.

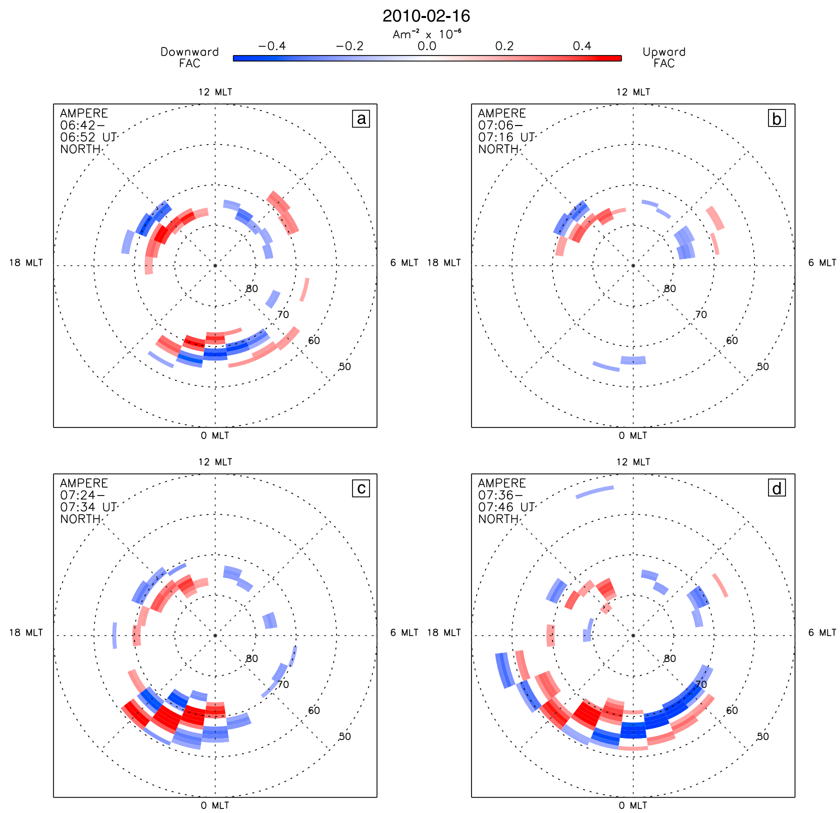

Figure 3. AMPERE-derived FACs for 16 February 2010 during selected 10 min time periods. Red denotes upward FAC, and blue denotes downward FAC. The FACs are plotted as a function of corrected geomagnetic latitude and magnetic local time with noon toward the top and midnight toward the bottom.

the time required for the constellation to sample the entire Northern or Southern Hemisphere. The onboard magnetometers have a temporal resolution of 20 s and a noise level on the order of 10 nT. These maps have a spatial resolution in geomagnetic coordinates of 1° in latitude and 1 h of magnetic local time (MLT) (15° in longitude), a temporal resolution of 2 min (by sliding the 10 min window each 2 min), and FAC resolution of ~0.1 μA (FAC amplitudes below this value or set to zero) [*Anderson et al.*, 2000; *Waters et al.*, 2001; *Murphy et al.*, 2012]. Note that the six orbital planes do not pass directly over the North Pole and precess with time such that nominal resolution in MLT can vary between approximately 1 and 3 h.

[8] In addition to FAC estimates provided by AMPERE, ground-based observations of the aurora and magnetic field perturbations during the substorm expansion phase provide complementary observations with which to infer the topology of ionospheric current systems. The THEMIS ASIs provided detailed observations of the aurora through the substorm expansion phase at 3 s cadence and measure auroral intensity as a function of counts [*Mende et al.*, 2008]. In this particular study we utilize the Northern Solar Terrestrial Array (NORSTAR) meridian scanning photometers (MSPs) to determine substorm onset times [*Donovan et al.*, 2003] at times when ASI observations of the aurora were not available. The MSPs have a 30 s cadence and measure auroral intensity in Rayleigh.

[9] Ground-based magnetometers can also be used to infer the location of regions of net upward and downward FAC in the ionosphere and the location and direction of ionospheric electrojets [*Clauer and McPherron*, 1974]. In this study we use auroral zone and low-latitude magnetometer data from the THEMIS [*Russell et al.*, 2008] and CARISMA [*Mann et al.*, 2008] magnetometer arrays to infer the azimuthal extent of the SCW and location of the upward and downward FAC elements [cf. *Lester et al.*, 1983; *Smith et al.*, 2002]. Ground-based magnetic field measurements are further supplemented by geosynchronous magnetic field measurements from GOES 11 and GOES 13 (G11 and G13) [*Singer et al.*, 1996]. Figure 1 shows the locations of the ground-based magnetometers, the fields of view of the ASIs and MSPs mapped to an altitude of 110 km used in this study and the north magnetic footprints of G11 and G13 traced with the T96 magnetic field model [*Tsyganenko*, 1995].

3. Observations

[10] In this section, we use three substorm case studies to characterize the development of the ionospheric currents and FAC systems coupling the ionosphere and magnetosphere through the substorm growth and expansion phases. Using data from the THEMIS ASIs, and for one case the NORSTAR MSPs, to define auroral substorm onset, we characterize the FAC topology associated with the SCW as inferred by AMPERE and develop a comprehensive two-dimensional view of the SCW. In addition, we demonstrate that regions of upward FAC are consistently associated with discrete auroral forms as viewed by the THEMIS ASIs, and the azimuthal

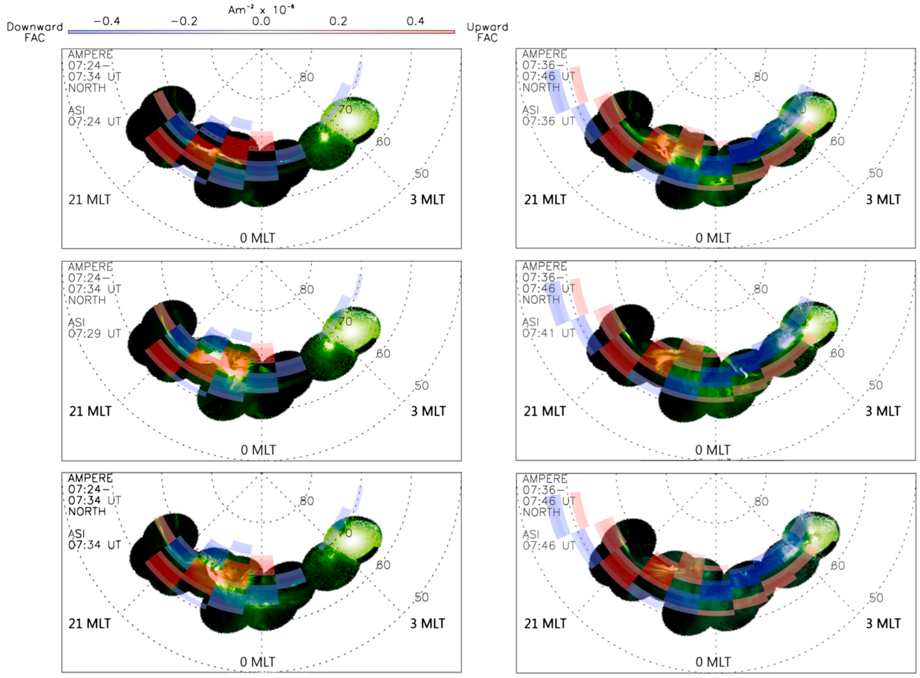

Figure 4. A superposition of the THEMIS ASI aurora observations and nightside FACs during the substorm expansion phase on 16 February 2010. The left column denotes the initial enhancement of the FAC system between 07:24 and 07:34 UT, and the right column denotes the subsequent evolution of the FAC system between 07:36 and 07:46. In each column, the three frames overplot the aurora at the beginning, middle, and end of the 10 min window encompassing the AMPERE-derived FACs (top, middle, and bottom frames, respectively).

extent of the SCW inferred from AMPERE is consistent with ground-based magnetometer observations.

3.1. The 16 February 2010 Event

[11] Figure 2 is an overview of an isolated substorm observed on 16 February 2010 from geosynchronous orbit (Figure 2a), three ground-based CARISMA magnetometers mapping to near geosynchronous L shells (Figures 2b–2d), and the THEMIS Fort Simpson (FSIM) ASI (Figure 2e). The FAC structure prior and local to the auroral onset region of this substorm was previously characterized in *Murphy et al.* [2012]. In this manuscript, we concentrate on the development of FACs following substorm onset and the structure of the SCW formed in the expansion phase rather than the evolution of the FACs and sequence of events leading to substorm onset. Fluctuations of the magnetic field are observed at 07:18 UT followed by a clear dipolarization of the magnetic field at 07:30 UT characterized by the sharp increase in the magnetic field strength (red) and inclination angle (the angle between the equatorial plane and the magnetic field vector; blue) of the geosynchronous magnetic field. Prior to the dipolarization, a sharp decrease in the geosynchronous magnetic field is observed coincident with the formation of ground magnetic bays and auroral onset at 07:18:30 UT of Figures 2b–2e. Figures 2b–2d show the north-south (*H*, blue), east-west (*D*, red), and vertical (*Z*, black) magnetic field perturbations from the Dawson City (DAWS), FSIM, and Fort Smith (FSMI) ground-based magnetometers, respectively. The magnetometers show a typical substorm response including the formation of magnetic bays [*Kisabeth and Rostoker*, 1971] and onset of large-amplitude ultralow frequency waves [*Olson*, 1999] associated with the substorm expansion phase and formation of the SCW. The largest bay structure is observed by the FSIM magnetometer closest to the auroral onset as illustrated by the FSIM ASI keogram (Figure 2e).

[12] The FSIM keogram (Figure 2e) was created by taking a slice through the FSIM ASI image perpendicular to the growth phase arc and in the local time sector of auroral onset. The resulting keogram shows a clear equatorward-propagating auroral arc typical of the growth phase [*Akasofu*, 1964]. Just prior to onset, a new equatorward arc formed at 07:06 UT, which briefly faded and finally brightened and expanded poleward at 07:18:30 UT, marking the onset of the substorm [cf. *Murphy et al.*, 2012].

[13] Figure 3 shows the evolution of the dayside and nightside FAC densities through the substorm growth and expansion phases as observed by AMPERE at four selected 10 min quasi-stationary time periods. As detailed in the previous section, sequential passes from satellites in the Iridium constellation allow quasi-stationary time periods in the magnetic field data to be identified. During these periods, we assume that any changes in the magnetic field represent spatial variations and thus can be used to determine the curl of the magnetic field required to infer FACs. Each panel of Figure 3 is plotted in magnetic local time (MLT) and corrected geomagnetic (CGM) latitude coordinates with noon at the top and midnight at the bottom. Red denotes upward FAC and blue denotes downward FAC. Between 0642 and 0652 UT shown in Figure 3a, AMPERE shows evidence of the dayside and nightside region 1 and region 2 current systems [cf., *Iijima and Potemra*, 1978]. Just prior to onset, at 07:06–07:16 UT

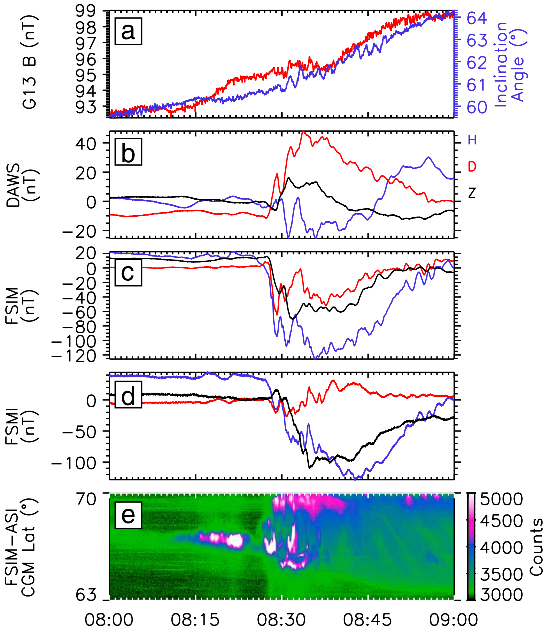

Figure 5. Summary of the geosynchronous magnetic field and ground-based magnetometer and ASI observations of a substorm on 24 March 2011. (a) The G13 total magnetic field (red) and inclination angle (blue). (b–c) DAWS, FSIM, and FSMI magnetograms in the same format as Figure 2. (e) FSIM keogram in the same format as Figure 2.

shown in Figure 3b, the nightside regions 1 and 2 current systems are significantly reduced [cf., *Murphy et al*., 2012] while the dayside region 1 and region 2 current systems remain relatively unchanged. Following auroral onset, the 07:24–07:34 UT and 07:36–07:46 UT frames, Figures 3c and 3d, respectively, show the development of structured upward and downward FACs between 60 and 75° CGM latitude. Initially, at 07:24–07:34 UT and shown in Figure 3c, the FAC elements form in the region of auroral onset, around 23 MLT and 68° CGM latitude, and subsequently, 0736–0746 UT in Figure 3d, expand azimuthally to span about 10 h of MLT.

[14] Figure 4 shows the AMPERE-derived expansion phase FAC system between 07:24–07:34 UT and 07:36–07:46 UT (left and right columns, respectively). Superimposed onto the FACs are the THEMIS ASI images at three select times: the beginning of the 10 min AMPERE window used to derive the FACs, the middle of the 10 min window, and the end of the 10 min window (top, middle, and bottom frames, respectively). Note that even over a 10 min period within the substorm expansion phase, during which the westward traveling surge forms and the aurora is extremely dynamic, the aurora is largely coincident with the upward FAC (red) regions as inferred by AMPERE. Regions of downward FAC are conversely typically devoid of discrete auroral forms or encompass more diffuse aurora.

3.2. The 24 March 2011 Event

[15] Figure 5, in the same format as Figure 2, is an overview of the geosynchronous magnetic field and ground-based observations of a substorm on 24 March 2011. Figure 5a shows the geosynchronous magnetic field and inclination angle at G13. Figures 5b–5d show the formation of the

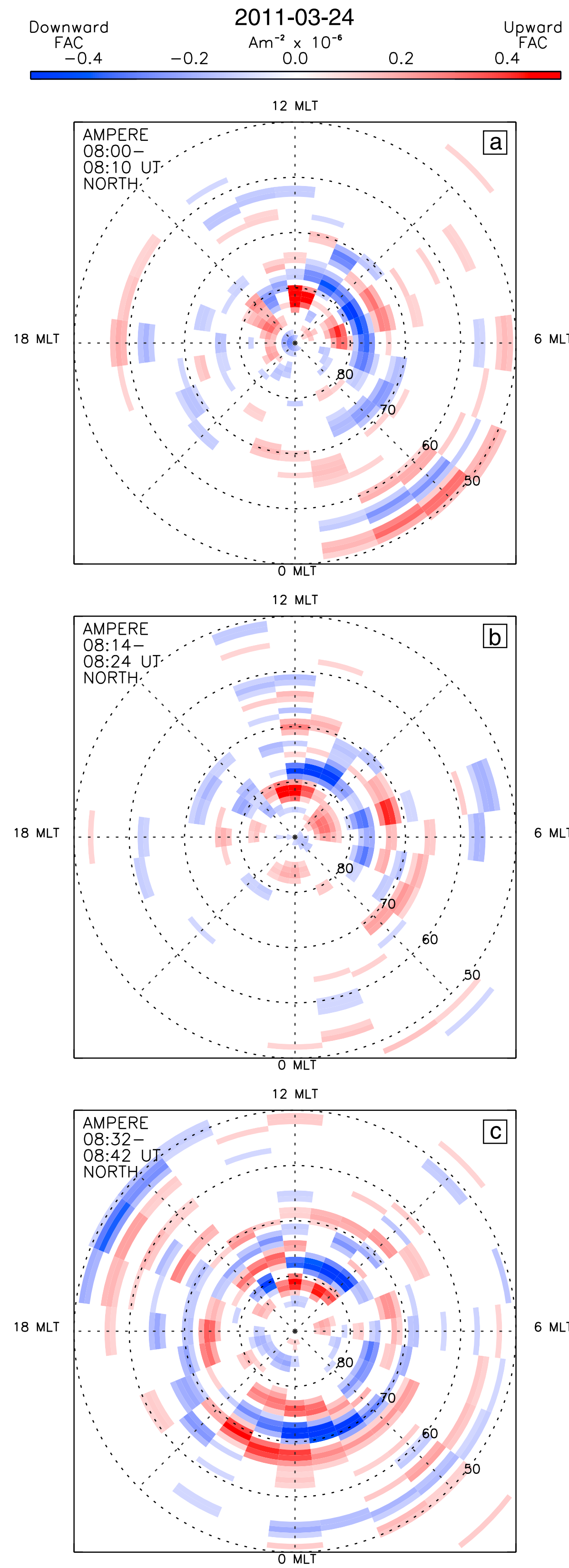

Figure 6. AMPERE-derived FACs during three time periods for the 24 March 2011 substorm. Red denotes upward FAC, and blue denotes downward FAC.

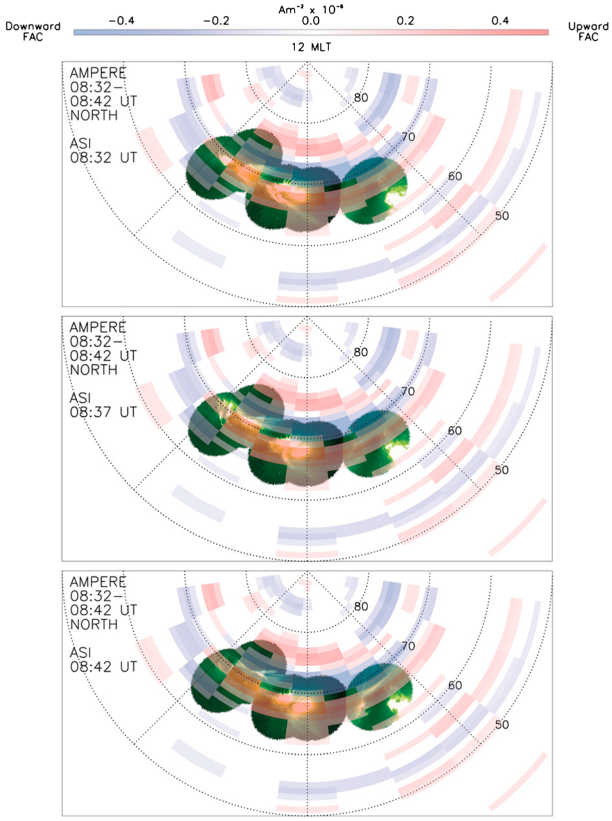

Figure 7. A superposition of the THEMIS ASI auroral observations and AMPERE-derived FACs for the 24 March 2011 substorm between 08:32 and 08:42 UT in the same format as Figure 4.

ground-based magnetic bays at DAWS, FSIM, and FSMI following substorm onset at 08:26:30 UT as illustrated in the FSIM keogram, Figure 5e. Prior to auroral onset and the formation of the magnetic bays, the FSIM keogram shows clear evidence of the substorm growth phase. The growth phase arc propagates equatorward [*Akasofu*, 1964], and just prior to onset, the arc dims [*Pellinen and Heikkila*, 1978; *Murphy et al.*, 2012] and then rapidly brightens and expands poleward characterizing the substorm expansion phase [*Akasofu*, 1964]. The geosynchronous magnetic field at G13 is nearly dipolar and shows little evidence of a dipolarization, although both the field strength and inclination angle increase following onset. There is however evidence of ultralow frequency (ULF) oscillations in both the G13 total magnetic field and the inclination angle following auroral onset likely in response to substorm expansion phase onset.

[16] Figure 6 shows the evolution of the AMPERE-derived FACs during three selected quasi-stationary 10 min time periods. The top and middle panels, 08:00–0810 UT and 08:14–08:24 UT, respectively, show the AMPERE FAC topology prior to auroral onset and the bottom panel, 08:32–08:42 UT, illustrates the FAC topology following onset. Between 08:00 and 08:10 UT, there is evidence of region 1 and region 2 current systems on the dawnside flank between 70° and 80° CGM latitude. On the nightside and duskside flank, the current systems are less well organized and there is no principal regions 1 and 2 current systems as defined by *Iijima and Potemra* [1978]. This may be the result of northward IMF throughout the duration of the event. The dawn flank continues to show evidence of the region 1 and region 2 current systems between 08:14 and 08:24 UT (Figure 6b). Just prior to auroral onset at 08:26:30 UT, the data in the midnight sector from Figure 6b show evidence of a decrease in the FAC density. The nightside FAC reduction occurs between 22–2 MLT and 60°–80° CGM latitude and is observed in a region conjugate to the subsequent auroral onset at 66° CGM latitude and 22.8 MLT [cf. *Murphy et al.*, 2012]. Following auroral onset, 08:32–08:42 UT, there is a clear increase in the strength of both the dayside and nightside currents during the substorm expansion phase.

[17] Similar to the previous substorm, an enhanced region of structured upward and downward FACs forms across midnight, following auroral onset, spanning about 22 MLT to nearly 4 MLT. Figure 7 highlights the relation between the aurora as observed by the THEMIS ASIs and the enhanced nightside current system forming during the substorm expansion phase. Similar to Figure 4, the ASI images are plotted with the AMPERE-derived FAC at the beginning, middle, and end of the 10 min AMPERE time window. Despite spanning a 10 min window, each panel shows remarkable correlation between regions of upward FAC and discrete aurora between 21–23 MLT and ~65°–70° CGM latitude. Similarly, the region of downward FAC, between 21–23 MLT and ~70°–75° CGM latitude, is nearly devoid of aurora.

3.3. The 16 May 2011 Event

[18] Figure 8 shows a summary of the geosynchronous and ground-based magnetic fields and auroral observations of a

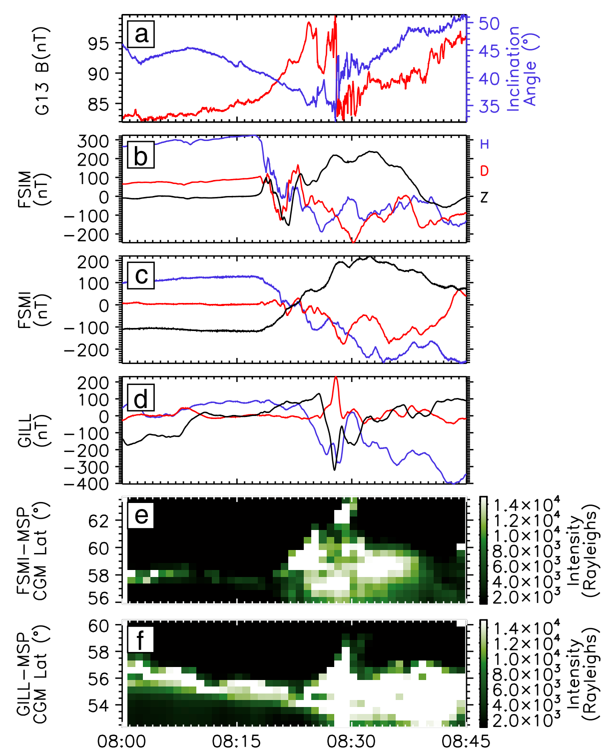

Figure 8. A summary of the 16 May 2011 substorm. (a) The G13 geosynchronous magnetic field (red) and inclination angle (blue). (b–d) FSIM, FSMI, and GILL magnetograms are in the same format as Figure 2. (e–f) Green line emissions from the FSMI and GILL NORSTAR MSPs.

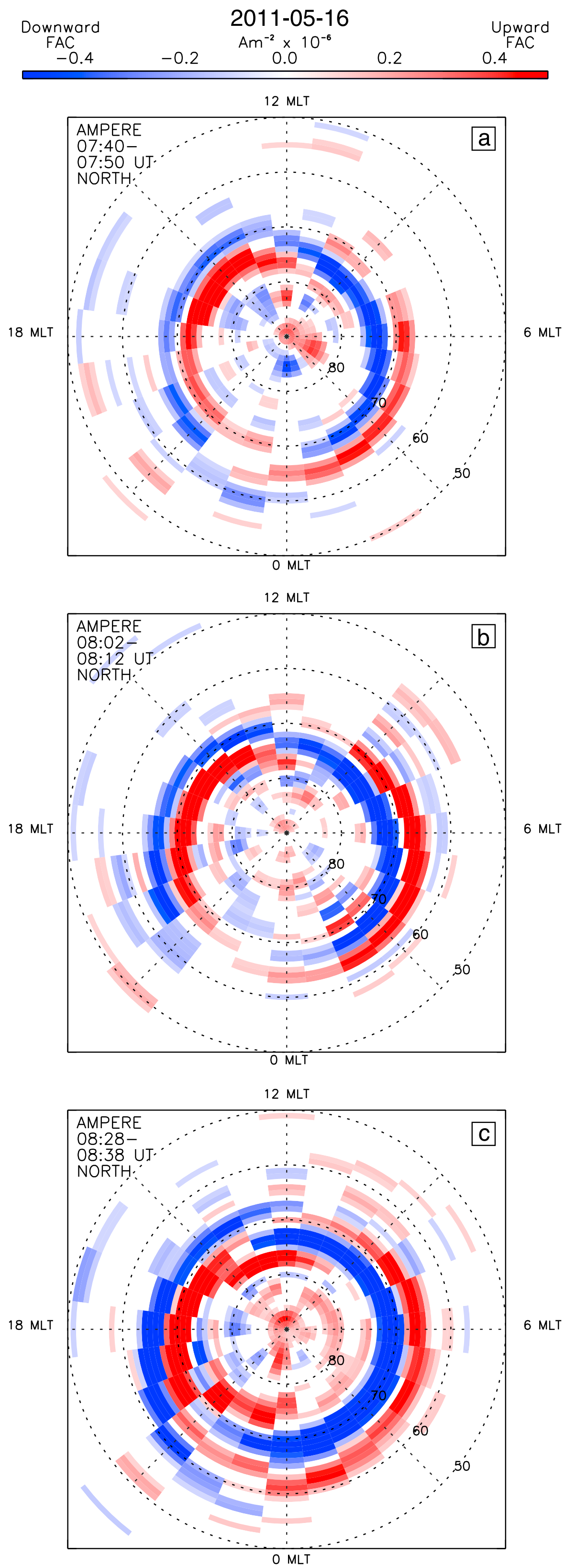

Figure 9. AMPERE-derived FACs for the 16 May 2011 substorm during selected periods in the same format as Figure 3.

substorm on 16 May 2011. For this particular substorm, there are limited auroral observations. Therefore, we use the Gillam (GILL) and FSMI MSP data from the NORSTAR to diagnose the auroral onset. The look directions of both MSPs are illustrated in Figure 1. The geosynchronous magnetic field shows a clear dipolarization of the field at 08:28 UT, depicted by the sharp increase in the inclination angle. Prior to the dipolarization, there is a compression of the geosynchronous magnetic field, illustrated by the increase in the magnetic field strength and decrease in the inclination angle between about 08:15 and 08:25 UT. During this time period, substorm bays begin to form in the FSIM, FSMI, and GILL magnetograms (Figures 8b–8d, respectively) and the aurora begins to expand poleward in the FSMI and GILL MSPs (Figures 8e–8f, respectively). The FSIM magnetometer shows the earliest evidence of substorm magnetic bay structure at ~08:17 UT as the *H* component (blue) begins to form a negative bay just before the aurora brightens and begins to move poleward at 08:20:30 UT as observed by the FSMI MSP.

[19] Figure 9, in the same format as Figures 3 and 6, show the AMPERE-derived FACs through the growth and expansion phase of the substorm. Throughout the growth phase, there is clear evidence of the region 1 and region 2 current systems on both the dayside and nightside, between 07:40 and 07:50 UT in Figure 9a, and a similar though enhanced pattern of currents is seen just prior to auroral onset, 08:02–08:12 UT in Figure 9b on the dayside. Similar to the previous two events, there is also evidence of a change in the FAC structure proceeding aurora onset. Initially, in Figure 9a, the 07:40–07:50 UT frame, the duskside low-latitude downward FAC (blue) extends to midnight and the high-latitude upward FAC (red) extends to 23 MLT. On the dawnside, the low-latitude upward FAC extends past midnight to 23 MLT and the upward FAC extends to 1 MLT. Just prior to onset, in Figure 9b, between 08:02 and 08:12 UT, these FAC structures undergo a clear and distinguished change. Both the upward and downward FAC structures on the duskside have withdrawn from the midnight meridian, and on the dawnside, the upward and downward FACs have a notable change in the strength of the current densities through the midnight meridian. Following substorm onset, between 08:28 and 08:38 UT in Figure 9c, a complex system of upward and downward FAC forms on nightside, between 23–1 MLT and 60°–80° CGM latitude.

3.4. The Substorm Current Wedge

[20] The nightside expansion phase FACs shown in Figures 4, 7, and 9c are all characteristic of the SCW. These current systems show the existence of small-scale FAC structures and are more complex than the simple equivalent current system of the SCW [*McPherron et al.*, 1973] and FACs described by *Iijima and Potemra* [1978]. Figure 10 shows the nightside FACs forming during the substorm expansion phase for each of the three substorms studied here. The left column of Figure 10 shows the AMPERE-derived FACs as well as the Pi2 ULF hodograms from selected low-latitude, middle-latitude, and auroral-latitude magnetometers. *Lester et al.* [1983] demonstrated that the direction of azimuth of Pi2 hodograms at low and middle latitudes can be used to infer the location of the upward and downward FAC elements and center of the SCW, while *Milling et al.* [2008] demonstrated the same polarization pattern of Pi2s in the auroral zone. The Pi2 hodograms shown in Figure 10 were determined from

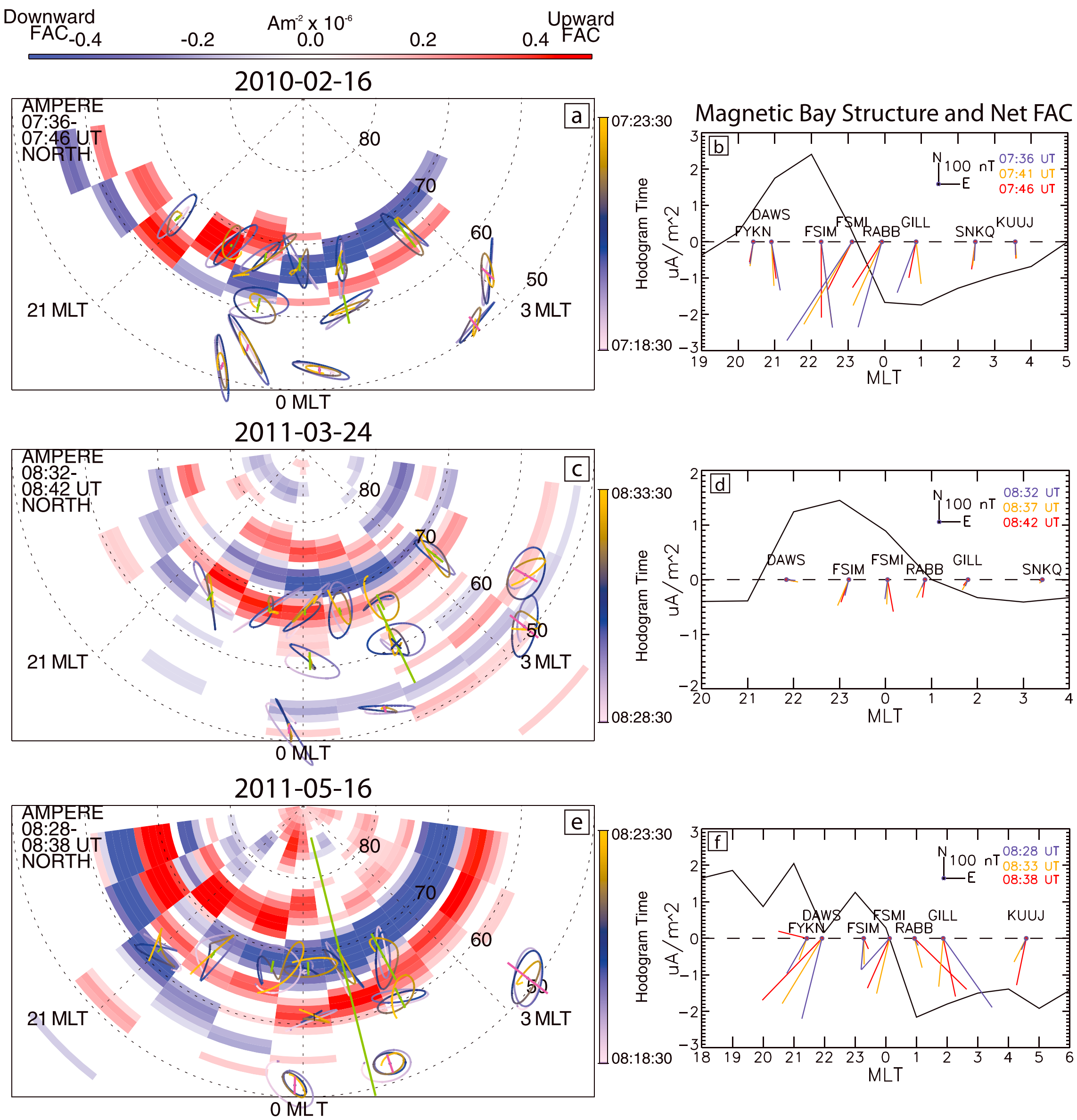

Figure 10. Left column: Nightside AMPERE-derived FACs during the substorm expansion phase for the three substorms. The Pi2 hodograms from selected auroral- and low-latitude magnetometer stations are overplotted. The vertical color bar denotes the time sequence of each hodogram, such that the color evolution in the hodograms allows the polarization sense (clockwise or counter clockwise) to be inferred. Right column: The latitudinal summation of the AMPERE FACs as a function of MLT for each of the two-dimension AMPERE FAC topologies shown in the left column (black line). The strength of the *H* and *D* components auroral zone magnetic bays at the beginning (blue), middle (yellow), and end (red) of each 10 min window used to derive the AMPERE FACs is superimposed on each panel. In the bays, positive *H* (north-south) points upward and positive *D* (east-west) points right as illustrated by the legend in the top right of each panel.

80 to 120 s period band-pass magnetograms following substorm onset. The color bar denotes the temporal evolution of each hodogram and the polarization sense. In each hodogram, *H* is magnetic north-south and *D* is magnetic east-west. The green line, or legend, represents 10 nT and the pink line represents 1 nT at auroral- and lower-latitude magnetometers, respectively. The center of each line marks the magnetometer location. Each hodogram and corresponding legend are independently scaled such that a smaller legend implies a larger Pi2 at that station and larger signal to noise ratio. Each legend is oriented in the north-south direction, pointing toward the geomagnetic pole.

[21] The right column of Figure 10 shows the net FAC as a function of MLT calculated by summing AMPERE FACs in latitude for each hour of MLT. The strength of the *H* and *D* component magnetic bays from auroral zone stations at the beginning (blue), middle (yellow), and end (red) of the 10 min AMPERE window are plotted as two-dimensional vectors along the *x* abscissa. The ground-based magnetic bays, formed as a result of the development of the SCW through the expansion phase, have distinct polarities based on the relative location of the magnetometer station to the longitudinal structure of the SCW, see for instance *Clauer and McPherron* [1974]

Figure 7 [see also *Smith et al*., 2002, Figure 8]. In each panel of the right column of Figure 10, the amplitude of the *H* and *D* magnetic bays is plotted to compare ground-based observations of the SCW with those from AMPERE, positive *H* and *D* pointing up and right, respectively.

[22] Both the right and left columns of Figure 10 support the *classical* view of the large-scale structure of the SCW. For each of the three substorms, the right column shows a net upward FAC premidnight and a net downward FAC post-midnight when the AMPERE FACs are integrated across latitude. Through the auroral zone, the ground-based magnetometers show the largest negative *H* bays in the region where the net FAC is nearly zero, i.e., through the expected center of the SCW. Through this region, there is also a clear reversal in the *D* magnetic bays, negative to the east and positive to the west. This picture of the relation between net FAC and the ground-based magnetic bays is consistent with those presented by *McPherron et al*. [1973] and *Smith et al*. [2002] using the equivalent line current model.

[23] The Pi2 hodograms also support the *classical* picture of the SCW. As demonstrated by *Lester et al*. [1983], inside the SCW, the semi-major axis (or angle of azimuth) of the Pi2 hodograms points toward the center of the wedge and outside the SCW, the semi-major axes point away from the center of the wedge such that there is a rotation of the semi-major axis across the center of the SCW and across the upward and downward FAC elements (cf. Figure 1 in *Lester et al*. [1984]). For each of the substorm events presented, the auroral zone and low-latitude hodograms show a rotation in the Pi2 hodogram azimuths consistent with that described by *Lester et al*. [1983].

[24] During the substorm on 16 February 2010, the auroral zone magnetometers show evidence of a reversal in the Pi2 azimuths between 21 and 22 MLT, the semi-major axis pointing west of north at ~21 MLT and east of north at ~22 MLT. No other clear reversal was observed in the auroral zone magnetometer data. At lower latitudes, the hodograms show another reversal in azimuth between magnetic midnight and ~1 MLT where the semi-major axis of the low-latitude magnetometer at ~53° points west of north and between 1 and 2 MLT the semi-major axis of the hodogram at ~61° points east of north. Together, the inferred location of the upward and downward FAC elements of the SCW from the ground-based Pi2 observations is between 21 and 22 MLT and magnetic midnight and 1 MLT, respectively. The location of the upward and downward FACs determined from the Pi2 hodograms is consistent with the net FAC illustrated in Figure 10b.

[25] On 24 March 2011, the Pi2 hodograms show a reversal of the semi-major axis in the auroral zone between 22 and 23 MLT and another reversal at both the auroral- and low-latitude magnetometers between 3 and 4 MLT. At 22 MLT, the semi-major axis at ~66° points west of north, and at 23 MLT, the semi-major axis at ~66° points east of north. In the morning sector, the semi-major axis auroral zone hodogram at ~66 and ~3 MLT points just slightly west of north. Conversely, the low-latitude hodograms between 3 and 4 MLT both have semi-major axes which point east of north. Together, these hodograms suggest that the upward FAC of the SCW lies between 22 and 23 MLT and downward FAC element lies between 3 and 4 MLT. These observations are consistent with the net FAC shown in Figure 10d.

[26] Finally, the hodograms on 5 May 2011 are more complicated than those of the two other substorms, especially in the auroral zone. The auroral zone does show evidence of a reversal in the azimuths of the hodograms between 1 and 2 MLT. At 1 MLT, the semi-major axis points west of north, and at 2 MLT, the semi-major axis points east of north. However, to the west, there is no clear evidence of any organized structure in the hodograms. Despite this, auroral zone hodograms between 1 and 2 MLT are characteristic of a region of downward FAC and consistent with a net downward FAC as shown in Figure 10f. It is important to note that *Lester et al*. [1984] showed that not all substorms follow the predicted polarization pattern and that during events with preexisting magnetic activity, the polarization patterns can become significantly more complicated making it difficult to infer the location of the upward and downward FAC elements of the SCW.

4. Discussion

[27] In this paper we have presented multisatellite observations of the FACs associated with the substorm growth and expansion phases and examine the two-dimensional structure and evolution of FACs in the SCW. FACs are inherently difficult to determine from in situ measurements, especially from single satellite, as the derivation of these currents assumes that a temporal observation of the magnetic field can be used to approximate spatial gradients in the field. For this reason, single-satellite inferences of FACs can be flawed as they are unable to separate spatial changes from temporal changes with single-point measurements. This space-time ambiguity can be removed using multispacecraft studies to identify quasi-stationary time periods during which temporal changes can be neglected. In this paper we use derived FAC distributions from AMPERE and the Iridium constellation of 70+ satellites, during quasi-stationary time periods for three substorms, to develop a comprehensive two-dimensional view of the FAC systems coupling the ionosphere and magnetosphere. As a result, we present the most detailed two-dimensional view of the structure of the FACs comprising the SCW to date. In particular, we show the following:

[28] 1. During the late growth phase and immediately prior to substorm onset, there is evidence of a change or reduction in the nightside FACs in the region of subsequent auroral substorm onset.

[29] 2. During the substorm expansion phase, regions of upward FACs are associated with discrete auroral forms. This demonstrates, for the first time, a two-dimensional correspondence between discrete aurora and upward FAC.

[30] 3. Following substorm expansion phase onset, an enhanced and highly structured system of upward and downward FACs forms on the nightside. When averaged over all latitudes, this complex current system reduces to what is typically described in terms of a simpler equivalent current system, the SCW.

[31] During the late growth phase, immediately preceding onset, discrete changes in the FAC density are observed on the nightside in each of the three substorms studied here. *Murphy et al*. [2012] discussed in detail the change in FAC observed during the 16 February 2010 substorm. We briefly restate those results here and demonstrate that similar changes are observed during both of the two other substorms.

For the 16 February 2010 case, Figure 3 shows a clear decrease in the FAC strength between the 06:42 and 06:52 UT frame and the 07:06–07:26 UT frame between 21–3 MLT and 63°–73° CGM latitude. During the 24 March 2011 substorm, a reduction in the FAC density in the region between 21–3 MLT and 60°–80° CGM latitude is observed between the 08:00–08:10 UT frame and the 08:14–08:24 UT frame as illustrated in Figure 6 . Although the 16 May 2011 substorm shows less drastic changes, there is still evidence of a change in the FAC densities and topology between the 07:40–07:50 UT and the 08:02–08:12 UT frames just prior to substorm onset in the premidnight sector between 60° and 70° CGM latitude.

[32] Previous observations have clearly shown the presence of wave activity in ground-based auroral images [*Elphinstone et al.*, 1995; *Donovan et al.*, 2008; *Liang et al.*, 2008; *Rae et al.*, 2010] with clear correlation between auroral waves and ground magnetic waves [e.g., *Rae et al.*, 2009a, 2009b, 2011, 2012] immediately prior to auroral substorm expansion phase onset and the formation of the SCW and westward traveling surge in the aurora. Moreover, *Newell et al.* [2010] showed a clear increase in wave-driven auroral particle precipitation in the minutes prior to substorm expansion phase onset. Recent observations of localized changes in the strength of nightside FACs prior to substorm onset suggest a key role for magnetosphere-ionosphere coupling in the late growth of a substorm [*Murphy et al.*, 2012]. The changes in FACs prior to substorm onset are likely mediated via the exchange of Alfvén waves between the magnetosphere and ionosphere prior to the traditional definition of substorm onset [*Murphy et al.*, 2012]. Such changes and related reduction in upward FACs may be manifested as auroral dimming preceding onset as illustrated in Figures 2e and 5e [see also *Pellinen and Heikkila*, 1978; *Baumjohann et al.*, 1981; *Murphy et al.*, 2012]. The formation of auroral beads [*Donovan et al.*, 2008; *Rae et al.*, 2009a, 2009b, 2010], potential characteristic of a near-Earth plasmasheet disturbance proceeding the substorm expansion phase [e.g., *Roux*, 1985; *Lui*, 1996; *Samson et al.*, 1996; *Maynard et al.*, 1996], may also be related to localized changed in the nightside FAC topology. With additional in situ instrumentation and ground-based observations, the detailed relationship between these features will be addressed further in future work. In any case, the observations of *Murphy et al.* [2012] considered together with those presented here provide important constraints to any substorm onset paradigm [cf. *Murphy et al.*, 2012].

[33] Following auroral substorm onset, during the substorm expansion phase, the FACs coupling the ionosphere to the magnetosphere undergo a radical topological change which is most notable on the nightside. However, there is evidence of enhanced FACs on the dayside as well. On the dayside, the region 1 and region 2 currents become enhanced and small-scale upward and downward FAC structures are observed in addition to the standard region 1 and region 2 current features (see Figures 3, 6, and 9). Whether this enhancement is the result of the substorm expansion phase or the effects of changes in solar wind driving is unclear. However, the enhancement of dayside FACs during the substorm expansion phase is consistent with the observations of *Rostoker et al.* [1982] who suggested that the nightside magnetotail currents can couple to the entire magnetosphere-ionosphere current system, including the dayside, through an enhanced auroral electrojet which forms during the substorm expansion phase.

[34] On the nightside, following auroral substorm onset, the FAC topology becomes highly structured and enhanced in each of the three substorms presented here. In each MLT sector, distinct azimuthal bands of upward and downward FAC form spanning at least 4 h of MLT and at times covering the entire nightside (larger than the separation of Iridium orbital planes) with periodic structuring in latitude (Figures 3, 4, 6, 7, and 9) [cf. *Inhester et al.*, 1981; *Gjerloev and Hoffman*, 2002]. These FAC structures are significantly more complicated than the equivalent line current system associated with the SCW [*McPherron et al.*, 1973] and the enhanced region 1 and 2 current system developed during active magnetospheric conditions [*Iijima and Potemra*, 1978]. However, when spatially averaged, these structured net upward and downward FACs depict the same line current SCW proposed by *McPherron et al.* [1973].

[35] FACs are inherently difficult to infer from in situ observations. Temporal variations in the magnetic field can lead to inaccurately derived FACs [*Peria et al.*, 2000; *Zheng et al.*, 2003; *Gjerloev et al.*, 2011]. *Zheng et al.* [2003] demonstrated using the Four Free-Flying Magnetometer payload of the Estrophy sounding rocket mission that the FAC density derived from multipoint measurements are typically smaller than those derived from single-point measurements. Similarly, using magnetometer data from the three ST 5 satellites, *Gjerloev et al.* [2011] showed that the correlation between multipoint magnetic field measurements decreases as a function of spacecraft separation. The magnetic fields are often not stationary in time over the duration of successive satellite passes. These studies clearly demonstrate that the further apart the observations, the more susceptible they are to spatiotemporal ambiguities which introduce errors into any derived FAC. In order to derive accurate FACs from in situ measurements, a constellation of closely spaced satellites is required to reduce the uncertainty introduced by a space-time ambiguity.

[36] In this study we have used quasi-stationary 10 min time periods defined by multiple nightside passes of satellites from the Iridium constellation to derive FAC estimates and determine the two-dimensional FAC topology during the substorm expansion phase. However, the substorm expansion phase is very dynamic. The aurora explosively expands forming the westward traveling surge, the magnetotail dipolarizes, and the auroral electrojets become enhanced. To verify that the AMPERE-derived FACs are an adequate representation of the FACs in the expansion phase, the derived FACs have been overplotted with auroral observations from THEMIS ASIs. Variability in auroral intensity in the THEMIS white light imagers is largely the result of the energy of precipitating electrons [*Mende et al.*, 2011, 2008]. Thus, by assuming that discrete aurora seen in the THEMIS ASI data is the result of precipitating electrons associated with upward FAC structures, we are able to validate the AMPERE-derived FACs and for the first time, verify that two-dimensional discrete arcs are identified by upward FAC structures.

[37] Figures 4 and 7 show the AMPERE FACs superimposed onto the THEMIS ASI data following substorms on 16 February 2010 and 24 March 2011, respectively. Both Figures 4 and 7 show a remarkable correlation between the THEMIS ASI auroral observations and derived AMPERE FACs. In each case, discrete auroral forms are principally

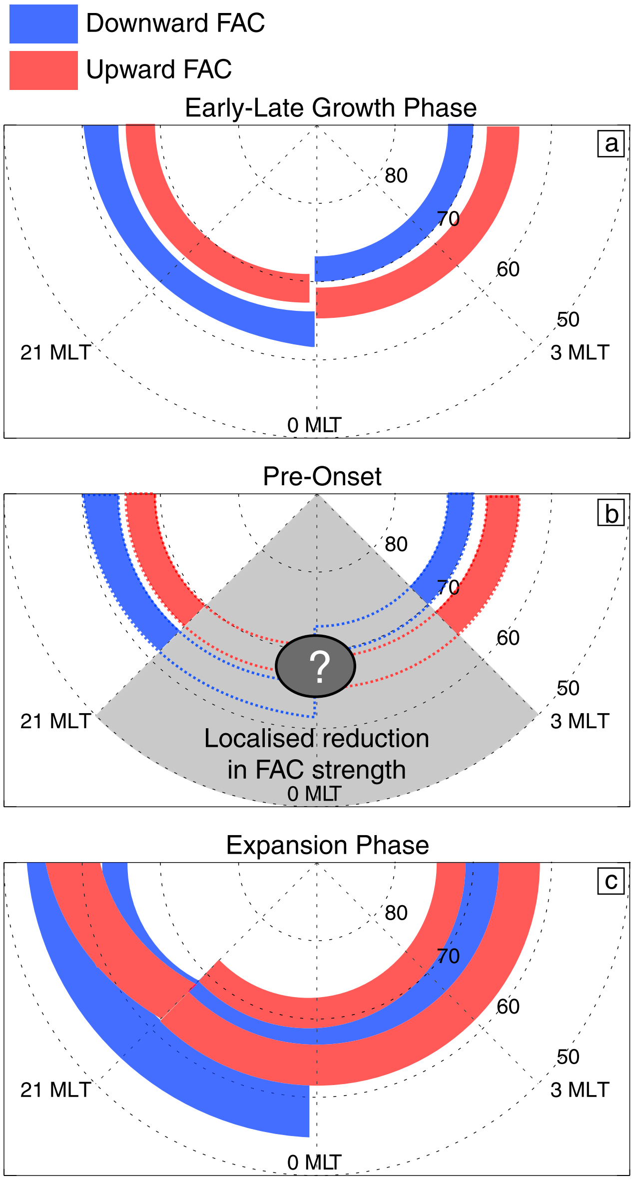

Figure 11. A schematic of the nightside FAC system during (a) the substorm growth phase,(b) prior to substorm onset, and (c) during the substorm expansion phase. In each panel, red denotes upward FAC and blue denotes downward FAC. Figure 11c is a schematic of the fine structure of the upward and downward FAC seen by AMPERE and which on a large scale composes the SCW FAC current system. Higher longitudinal resolution studies are needed to resolve the onset region in Figure 11b.

associated with regions of upward FAC in the premidnight sector. The largest discrepancy is in the final two auroral frames in Figure 4 (left column). A discrete auroral arc expands westward along the boundary between the upward and downward FACs at 21 MLT and 66° CGM latitude and back into a region of upward FAC at 22 MLT. This may be the result of local changes in the magnetic field and auroral precipitation and specifically, the poleward motion of the aurora during the expansion phase, leading to a localized breakdown in the quasi-stationary assumption used to derive FACs and an incorrectly derived location of the region of upward FAC over the 10 min time period. Despite this small discrepancy, overall, Figures 4 and 7 demonstrate a remarkable relation between the AMPERE-derived upward FACs and discrete aurora seen in the THEMIS ASI data during the substorm expansion phase. Not only do these observations verify the accuracy of the derived location and structure of the FACs from AMPERE and Iridium but they also provide the first observations of a two-dimensional correspondence between discrete aurora and upward FAC.

[38] *Gelpi et al.* [1987] demonstrated, using both in situ magnetic field and auroral observations and ground-based magnetometer observations, that the head of the westward traveling surge was associated with upward FAC. Similarly, using FAST satellite passes through a single meridian of the westward traveling surge (WTS) identified by auroral observations from the Imager for Magnetopause-to-Aurora Global Exploration spacecraft, *Mende et al.* [2003a, 2003b] demonstrated that the WTS is characteristic of intense upward FACs and precipitating electrons. Using ground-based auroral cameras and the FAST spacecraft, *Dubyagin et al.* [2003] have further shown that the substorm onset arc is embedded in a region of upward FAC. Our results are consistent with *Mende et al.* [2003a, 2003b] and *Dubyagin et al.* [2003]. However, we extend these results for the first time to two-dimensions demonstrating a clear correspondence between discrete aurora and upward FAC over an extended range of latitude and MLT during the substorm expansion phase.

[39] While the nightside current systems that form during the substorm expansion phase are more complex than the equivalent line current system [*McPherron et al.*, 1973], Figure 10 clearly demonstrates that these current systems are characteristic of the SCW for each case study shown. The structured FACs illustrated in Figure 10 are consistent with auroral observations from the THEMIS ASI data, the ground-based Pi2 hodograms, and the ground-based magnetic bays forming as a result of the overhead SCW. Based on the three case study observations presented here, in Figure 11, we present an idealized schematic of the FAC topology seen by AMPERE during the substorm sequence. Figures 11a–11c show the growth phase, just prior to substorm onset and during the substorm expansion phase. During the substorm growth phase, the FAC system is characteristic of an enhanced region 1/region2 current system (cf., Figure 11a). This enhanced current system is characteristic of the enhanced magnetospheric and ionospheric currents developing during substorm growth phase [*McPherron*, 1970] under active magnetospheric conditions [*Iijima and Potemra*, 1978] and also observed statistically by AMPERE pre-onset by *Clausen et al.* [2013]. Following the substorm growth phase and just prior to auroral onset, the nightside FACs undergo a distinct topological change, Figure 11b. The shaded grey region in Figure 11b highlights the region surrounding magnetic midnight where substorm onset typically occurs, and the small circle characterizes the localized change in FACs associated with substorm onset. *Murphy et al.* [2012] discussed highlighting an important role for magnetosphere-ionosphere coupling at substorm onset. However, more work is required in order to fully understand the change in FACs and examine in detail the pre-onset changes in magnetosphere-ionosphere coupling prior to auroral onset and their association with the SCW. Hence, in Figure 11b, we only note that there is a change in nightside FACs preceding auroral onset. Following substorm expansion phase onset, a

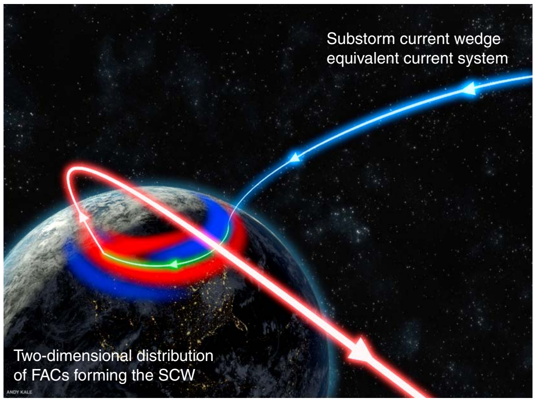

Figure 12. A schematic of the two-dimensional FACs forming during the substorm expansion phase, and the equivalent current system forming the SCW. The blue, green, and red arrows represent the net upward FAC, the enhanced westward electrojet, and the net upward FAC of the SCW. The azimuthal bands of upward and downward FAC, red and blue, respectively, illustrate the complex structure of FACs forming during the expansion phase and comprising the SCW.

series of azimuthally banded and latitudinally periodic upward and downward FACs form across the nightside, Figure 11c. This nightside FAC topology is in fact the detailed two-dimensional structure of the SCW [cf., *Gjerloev and Hoffman*, 2002; *Birn et al*., 2011].

[40] The original descriptions of the SCW equivalent current system as a downward FAC element in the east, an enhanced westward electrojet, and an upward FAC element in the west were derived from ground-based magnetometer observations [*McPherron et al*., 1973]. The FAC topology illustrated in Figure 11c has the same equivalent current distribution as that described by *McPherron et al*. [1973], a net downward FAC in the east and net upward FAC in the west (cf. Figure 10). However, with the increased spatial resolution of the AMPERE in situ observations, we are able to derive a more detailed view of the SCW and detail potentially critical aspects of magnetosphere-ionosphere coupling during substorms. Figure 12 is a schematic of the two-dimensional FACs forming during the substorm expansion phase. The azimuthal bands of upward and downward FAC, red and blue, respectively, illustrate the complex structure of FACs forming during the expansion phase and comprising the SCW. Superimposed onto these FACs is the simplified SCW equivalent current system; blue, the net downward FAC; red, the net upward FAC; and green, the enhanced westward electrojet. Note that the FAC sheets do not necessarily close solely through the enhanced electrojet depicted by the green arrow but more likely through a complex system of Hall and Pedersen currents throughout the SCW.

[41] Using single-satellite passes through the auroral zone, *Rostoker et al*. [1975] demonstrated that an intense region of upward FAC formed along the enhanced ionospheric electrojets surrounded to the north and south by regions of downward FAC following substorm onset which is similar to our AMPERE results. Using single-satellite passes through the auroral zone, *Iijima and Potemra* [1978] compiled a statistical study of TRIAD passes to develop a statistical view of the FAC topology during active magnetospheric conditions. These authors concluded that the region 1 and region 2 current systems persisted during active magnetospheric conditions, although in the region of the Harang discontinuity, the currents were significantly more complex. During moderately active conditions, *Iijima and Potemra* [1978] found evidence of a current system similar to that described by *Rostoker et al*. [1975], whereas during very active conditions, the currents were very complicated, exhibiting fine-scale variations. The current systems described by *Rostoker et al*. [1975] and *Iijima and Potemra* [1978] are consistent with the equivalent current system described by *McPherron et al*. [1973] and with the SCW schematic shown in Figure 11c. The upward FAC surrounded by downward FACs at higher and lower latitudes [cf. *Rostoker et al*., 1975; *Iijima and Potemra*, 1978] is similar to the FAC topology forming in the postmidnight sector. In the premidnight sector, however, a more complicated current system forms following substorm onset and there is no evidence of the distinct region 1 and region 2 current systems as described by *Iijima and Potemra* [1978].

[42] The differences between the premidnight current system described here and the current systems described by *Rostoker et al*. [1975] and *Iijima and Potemra* [1978] likely result from comparing single-satellite case and statistical studies to the more accurate description of FAC structure obtained from multisatellite studies presented here. *Iijima and Potemra* [1978] developed a two-dimensional distribution of FACs by spatially averaging large-scale FACs from multiple passes of the TRIAD satellite through the auroral zone. This averaging will obscure small-scale spatial structures, producing a smoothed distribution of FACs in both MLT and latitude. In this study we have derived the schematic illustrated in Figure 11c using two-dimensional multisatellite coverage from three case studies. In each case study we were able to determine the full two-dimensional distribution of FACs, rather than relying on a statistical average. Therefore, the schematic illustrated in Figure 11 is not subject to any spatial smoothing and is expected to be a more accurate representation of the FAC current topology during the substorm cycle.

[43] In each of the substorms studied, the complex nightside FAC system formed in the expansion phase developed during auroral breakup and in two cases during the dipolarization of the geosynchronous magnetic field. Thus, the inward convection of electrons [*Vasyliunas*, 1968], onset of fast flows [*Angelopoulos et al*., 1992], and development of dipolarization fronts [*Runov et al*., 2008] following tail reconnection are likely to be intimately linked to the development of the current system depicted in Figure 11c.

[44] *Yao et al*. [2012] recently demonstrated that the azimuthal divergence or deceleration of fast flows in the tail observed during the substorm expansion phase produced a FAC current signature consistent with the equivalent current system described by *McPherron et al*. [1973]. Our AMPERE-derived observations of the net FAC as a function of MLT are consistent with the observations of *Yao et al*. [2012]. The two-dimensional AMPERE FAC distributions show latitudinal and azimuthal structuring in the form of discrete upward and downward FAC current sheets. *Birn et al*. [1999] demonstrated that the braking of earthward flows contributed to the initial formation of the SCW but that the more dominant and permanent current contributions where the result of pressure gradients. Further, *Mende et al*. [2003b] concluded that high-energy

precipitating electrons energized by Alfvén waves driven by the dipolarization of the field or reconnection at the near-Earth neutral line are responsible for part of the current forming in the westward traveling surge. The FAC current system developing during the substorm expansion phase illustrated in Figure 11c is a superposition of all the current forming during the substorm expansion phase. Therefore, it is not surprising that the current system is more complicated than that described by *McPherron et al*. [1973] or that illustrated in *Yao et al*. [2012]. Indeed, we have demonstrated that expansion phase FAC current system is very well correlated with the expansion phase aurora and forms following auroral breakup and dipolarization of the tail. Though this current system is more complex than the classical view of the SCW, it is fully consistent with the equivalent current system described by *McPherron et al*. [1973] (see schematic in Figure 12).

5. Summary and Conclusions

[45] The substorm current wedge has historically been viewed using an equivalent current system compozsed of a downward FAC element in the dawn sector, an enhanced westward electrojet, and an upward FAC element in the dusk sector [*McPherron et al*., 1973]. In this manuscript we have used in situ measurements from the low Earth-orbiting Iridium constellation and the AMPERE mission [*Anderson et al*., 2000; *Waters et al*., 2001] to characterize in more detail the two-dimensional FAC system coupling the ionosphere to the magnetosphere during the substorm growth and expansion phases. These results are only possible using multipoint measurements available via AMPERE.

[46] In particular, we have demonstrated that several minutes prior to substorm onset, there is a localized change or reduction in the nightside FAC system which was described by *Murphy et al*. [2012] and which represents a change in the magnetosphere-ionosphere coupling before onset. Following substorm onset, a complex and highly structured system of FACs forms on the nightside (Figure 12). The upward FAC elements of this intricate FAC system are correlated with discrete aurora during the expansion phase. This demonstrates for the first time a two-dimensional correspondence between upward FAC structures and discrete aurora. Although more complex than the equivalent line current system comprising the SCW, the structured FAC system we report here and which form during the substorm expansion phase is fully consistent with that described by *McPherron et al*. [1973] and with ground-based observations of the SCW during the expansion phase [*Lester et al*., 1983; *Smith et al*., 2002] if it is integrated over all latitudes to show the net upward and downward FAC as a function of MLT. Finally, we present a detailed schematic of the FACs through the substorm growth and expansion phases, Figures 11 and 12, and note that the complexity of the currents suggests future work should address the effects of multiple nightside FAC sources to explain the observed morphology of the SCW.

[47] **Acknowledgments.** K.R.M. is funded by an Alberta Innovates Graduate Scholarship. I.R.M is supported by a Discovery Grant from NSERC, and I.J.R. is funded by the Canadian Space Agency (CSA). We thank the AMPERE team and the AMPERE Science Center for providing the Iridium-derived data products. We acknowledge NASA contract NAS5-02099 and V. Angelopoulos for use of data from the THEMIS Mission and NSF support of GIMNAST through grant AGS-1004736. Specifically, we thank S. Mende and E. Donovan for use of the THEMIS ASI data. Deployment and data retrieval of the THEMIS ASIs were partly supported by CSA contract 9 F007-046101 to the University of Calgary. We thank S. Mende and C.T. Russell for the use of the THEMIS ground-based magnetometer data and NSF for support through grant AGS-1004814. Operational support for NORSTAR is provided by the CSA and University of Calgary. We acknowledge Brian Jackel and the NORSTAR team for providing the MSP data used in this study. We acknowledge D.K. Milling and the rest of the CARISMA team for data use. CARISMA is operated by the University of Alberta, funded by the CSA.

[48] Robert Lysak thanks Mark Lester and an anonymous reviewer for their assistance in evaluating this paper.

References

Akasofu, S. I. (1964), The development of the auroral substorm, *Planet. Space Sci.*, *12*, 273–282.

Anderson, B. J., K. Takahashi, and B. A. Toth (2000), Sensing global Birkeland currents with Iridium® engineering magnetometer data, *Geophys. Res. Lett.*, *27*(24), 4045–4048, doi:10.1029/2000GL000094.

Angelopoulos, V., W. Baumjohann, C. F. Kennel, F. V. Coroniti, M. G. Kivelson, R. Pellat, R. J. Walker, H. Lühr, and G. Paschmann (1992), Bursty bulk flows in the inner central plasma sheet, *J. Geophys. Res.*, *97*(A4), 4027–4039, doi:10.1029/91JA02701.

Baumjohann, W., R. J. Pelunen, H. J. Opgenoorth, and E. Nielsen (1981), Joint two-dimensional observations of ground magnetic and ionospheric electric fields associated with auroral zone currents: Current systems associated with local auroral break-ups, *Planet. Space Sci.*, *29*(4), 431–447, doi:10.1016/0032-0633(81)90087-8.

Birn, J., M. Hesse, G. Haerendel, W. Baumjohann, and K. Shiokawa (1999), Flow braking and the substorm current wedge, *J. Geophys. Res.*, *104*(A9), 19,895–19,903.

Birn, J., R. Nakamura, E. V. Panov, and M. Hesse (2011), Bursty bulk flows and dipolarization in MHD simulations of magnetotail reconnection, *J. Geophys. Res.*, *116*, A01210, doi:10.1029/2010JA016083.

Clauer, C., and R. McPherron (1974), Mapping the local time-universal time development of magnetospheric substorms using mid-latitude magnetic observations, *J. Geophys. Res.*, *79*(19), 2811–2820.

Clausen, L. B. N., J. B. H. Baker, J. M. Ruohoniemi, S. E. Milan, J. C. Coxon, S. Wing, S. Ohtani, and B. J. Anderson (2013), Temporal and spatial dynamics of the regions 1 and 2 Birkeland currents during substorms, *J. Geophys. Res. Space Physics*, *118*, 3007–3016, doi:10.1002/jgra.50288.

Cummings, W., J. Barfield, and P. Coleman Jr. (1968), Magnetospheric substorms observed at the synchronous orbit, *J. Geophys. Res.*, *73*(21), 6687–6698.

Donovan, E. F., T. S. Trondsen, L. L. Cogger, and B. J. Jackel (2003), All-sky imaging within the Canadian CANOPUS and NORSTAR projects, *Sodankyla Geophys. Obs. Publ.*, *92*, 109–112.

Donovan, E., et al. (2008), Simultaneous THEMIS in situ and auroral observations of a small substorm, *Geophys. Res. Lett.*, *35*, L17S18, doi:10.1029/2008GL033794.

Dubyagin, S. V., V. A. Sergeev, C. W. Carlson, S. R. Marple, T. I. Pulkkinen, and A. G. Yahnin (2003), Evidence of near-Earth breakup location, *Geophys. Res. Lett.*, *30*(6, 1282), doi:10.1029/2002GL016569.

Elphinstone, R. D., et al. (1995), The double oval UV auroral distribution: 1. Implications for the mapping of auroral arcs, *J. Geophys. Res.*, *100*(A7), 12,075–12,092, doi:10.1029/95JA00326.

Gelpi, C., H. J. Singer, and W. J. Hughes (1987), A comparison of magnetic signatures and DMSP auroral images at substorm onset: Three case studies, *J. Geophys. Res.*, *92*(A3), 2447–2460, doi:10.1029/JA092iA03p02447.

Gjerloev, J. W., and R. A. Hoffman (2002), Currents in auroral substorms, *J. Geophys. Res.*, *107*(A8, 1163), doi:10.1029/2001JA000194.

Gjerloev, J. W., S. Ohtani, T. Iijima, B. Anderson, J. Slavin, and G. Le (2011), Characteristics of the terrestrial field-aligned current system, *Ann. Geophys.*, *29*, 1713–1729, doi:10.5194/angeo-29-1713-2011.

Iijima, T., and T. A. Potemra (1976), The amplitude distribution of field-aligned currents at northern high latitudes observed by Triad, *J. Geophys. Res.*, *81*(13), 2165–2174, doi:10.1029/JA081i013p02165.

Iijima, T., and T. A. Potemra (1978), Large-scale characteristics of field-aligned currents associated with substorms, *J. Geophys. Res.*, *83*(A2), 599–615, doi:10.1029/JA083iA02p00599.

Inhester, B., W. Baumjohann, R. A. Greenwald, and E. Nielsen (1981), Joint two-dimensional observations of ground magnetic and ionospheric electric fields associated with auroral zone currents. 3: Auroral zone currents during the passage of a westward traveling surge, *J. Geophys.*, *49*, 155–162.

Kisabeth, J. L., and G. Rostoker (1971), Development of the polar electrojet during polar magnetic substorms, *J. Geophys. Res.*, *76*(28), 6815–6828, doi:10.1029/JA076i028p06815.

Lester, M., W. J. Hughes, and H. J. Singer (1983), Polarization patterns of Pi 2 magnetic pulsations and the substorm current wedge, *J. Geophys. Res.*, *88*(A10), 7958–7966.

Lester, M., W. J. Hughes, and H. J. Singer (1984), Longitudinal structure in Pi 2 pulsations and the substorm current wedge, *J. Geophys. Res.*, *89*(A7), 5489–5494, doi:10.1029/JA089iA07p05489.

Liang, J., E. F. Donovan, W. W. Liu, B. Jackel, M. Syrjäsuo, S. B. Mende, H. U. Frey, V. Angelopoulos, and M. Connors (2008), Intensification of preexisting auroral arc at substorm expansion phase onset: Wave-like disruption during the first tens of seconds, *Geophys. Res. Lett.*, *35*, L17S19, doi:10.1029/2008GL033666.

Lui, A. T. Y. (1996), Current disruption in the Earth's magnetosphere: Observations and models, *J. Geophys. Res.*, *101*(A6), 13,067–13,088, doi:10.1029/96JA00079.

Mann, I. R., et al. (2008), The upgraded CARISMA magnetometer array in the THEMIS era, *Space Sci. Rev.*, *141*, 413–451, doi:10.1007/s11214-008-9457-6.

Maynard, N. C., W. J. Burke, E. M. Basinska, G. M. Erickson, W. J. Hughes, H. J. Singer, A. G. Yahnin, D. A. Hardy, and F. S. Mozer (1996), Dynamics of the inner magnetosphere near times of substorm onsets, *J. Geophys. Res.*, *101*(A4), 7705–7736, doi:10.1029/95JA03856.

McPherron, R. L. (1970), Growth phase of magnetospheric substorms, *J. Geophys. Res.*, *75*(28), 5592–5599, doi:10.1029/JA075i028p05592.

McPherron, R. L., C. T. Russell, and M. P. Aubry (1973), Satellite studies of magnetospheric substorms on August 15, 1968: 9. Phenomenological model for substorms, *J. Geophys. Res.*, *78*(16), 3131–3149, doi:10.1029/JA078i016p03131.

Mende, S. B., C. W. Carlson, H. U. Frey, L. M. Peticolas, and N. Østgaard (2003a), FAST and IMAGE-FUV observations of a substorm onset, *J. Geophys. Res.*, *108*(A9, 1344), doi:10.1029/2002JA009787.

Mende, S. B., C. W. Carlson, H. U. Frey, T. J. Immel, and J.-C. Gérard (2003b), IMAGE FUV and in situ FAST particle observations of substorm aurorae, *J. Geophys. Res.*, *108*(A4, 8010), doi:10.1029/2002JA009413.

Mende, S. B., S. E. Harris, H. U. Frey, V. Angelopoulos, C. T. Russell, E. Donovan, B. Jackel, M. Greffen, and L. M. Peticolas (2008), The THEMIS array of ground-based observatories for the study of auroral substorms, *Space Sci. Rev.*, *141*, 357–387.

Mende, S. B., H. U. Frey, V. Angelopoulos, and Y. Nishimura (2011), Substorm triggering by poleward boundary intensification and related equatorward propagation, *J. Geophys. Res.*, *116*, A00I31, doi:10.1029/2010JA015733.

Milling, D. K., I. J. Rae, I. R. Mann, K. R. Murphy, A. Kale, C. T. Russell, V. Angelopoulos, and S. Mende (2008), Ionospheric localisation and expansion of long-period Pi1 pulsations at substorm onset, *Geophys. Res. Lett.*, *35*, L17S20, doi:10.1029/2008GL033672.

Murphy, K. R., I. R. Mann, I. J. Rae, C. L. Waters, B. J. Anderson, D. K. Milling, H. J. Singer, and H. Korth (2012), Reduction in field-aligned currents preceding and local to auroral substorm onset, *Geophys. Res. Lett.*, *39*, L15106, doi:10.1029/2012GL052798.

Newell, P. T., A. R. Lee, K. Liou, S.-I. Ohtani, T. Sotirelis, and S. Wing (2010), Substorm cycle dependence of various types of aurora, *J. Geophys. Res.*, *115*, A09226, doi:10.1029/2010JA015331.

Olson, J. V. (1999), Pi2 pulsations and substorm onsets: A review, *J. Geophys. Res.*, *104*(A8), 17,499–17,520, doi:10.1029/1999JA900086.

Pellinen, R. J., and W. J. Heikkila (1978), Observations of auroral fading before breakup, *J. Geophys. Res.*, *83*(A9), 4207–4217, doi:10.1029/JA083iA09p04207.

Peria, W. J., C. W. Carlson, R. E. Ergun, J. P. McFadden, J. Bonnell, R. C. Elphic, and R. J. Strangeway (2000), Characteristics of field-aligned currents near the auroral acceleration region: FAST observations, in *Magnetospheric Current Systems*, Geophys. Monogr. Ser., vol. *118*, edited by S. Ohtani et al., pp. 181–189, AGU, Washington, D. C., doi:10.1029/GM118p0181.

Rae, I. J., et al. (2009a), Near-Earth initiation of a terrestrial substorm, *J. Geophys. Res.*, *114*, A07220, doi:10.1029/2008JA013771.

Rae, I. J., et al. (2009b), Timing and localization of ionospheric signatures associated with substorm expansion phase onset, *J. Geophys. Res.*, *114*, A00C09, doi:10.1029/2008JA013559.

Rae, I. J., C. E. J. Watt, I. R. Mann, K. R. Murphy, J. C. Samson, K. Kabin, and V. Angelopoulos (2010), Optical characterization of the growth and spatial structure of a substorm onset arc, *J. Geophys. Res.*, *115*, A10222, doi:10.1029/2010JA015376.

Rae, I. J., K. R. Murphy, C. E. J. Watt, and I. R. Mann (2011), On the nature of ULF wave power during nightside auroral activations and substorms: 2. Temporal evolution, *J. Geophys. Res.*, *116*, A00I22, doi:10.1029/2010JA015762.

Rae, I. J., C. E. J. Watt, K. R. Murphy, H. U. Frey, L. G. Ozeke, D. K. Milling, and I. R. Mann (2012), The correlation of ULF waves and auroral intensity before, during and after substorm expansion phase onset, *J. Geophys. Res.*, *117*, A08213, doi:10.1029/2012JA017534.

Rostoker, G., J. C. Armstrong, and A. J. Zmuda (1975), Field-aligned current flow associated with intrusion of the substorm-intensified westward electrojet into the evening sector, *J. Geophys. Res.*, *80*(25), 3571–3579, doi:10.1029/JA080i025p03571.

Rostoker, G., M. Mareschal, and J. C. Samson (1982), Response of dayside net downward field-aligned current to changes in the interplanetary magnetic field and to substorm perturbations, *J. Geophys. Res.*, *87*(A5), 3489–3510, doi:10.1029/JA087iA05p03489.

Roux, A. (1985), Generation of field-aligned current structures at substorm onsets, in *Proceedings of ESA Workshop on Future Missions in Solar, Heliospheric and Space Plasma Physics*, Spec. Publ., ESA SP-235, pp. 151–159 , Eur. Space Agency, Garmisch-Partenkirchen, Germany.

Runov, A., et al. (2008), Multipoint in situ and ground-based observations during auroral intensifications, *J. Geophys. Res.*, *113*, A00C07, doi:10.1029/2008JA013493.

Russell, C. T., P. J. Chi, D. J. Dearborn, Y. S. Ge, B. Kuo-Tiong, J. D. Means, D. R. Pierce, K. M. Rowe, and R. C. Snare (2008), THEMIS ground-based magnetometers, *Space Sci. Rev.*, *141*, 389–412, doi:10.1007/s11214-008-9337-0.

Samson, J. C., et al. (1996), Substorm intensifications and resistive shear flow-ballooning instabilities in the near-Earth magnetotail, in *Proceedings of the Third International Conference on Substorms (ICS-3)*, Spec. Publ., ESA SP-389, pp. 399–404 , Eur. Space Agency, Versailles, France.

Singer, H. J., L. Matheson, R. Grubb, A. Newman, and S. D. Bouwer (1996), Monitoring space weather with the GOES magnetometers, *Proc. SPIE Int. Soc. Opt. Eng.*, *2812*, 299–308.

Smith, A. J., M. P. Freeman, S. Hunter, and D. K. Milling (2002), VLF, magnetic bay, and Pi2 substorm signatures at auroral and mid-latitude ground stations, *J. Geophys. Res.*, *107*(A12, 1439), doi:10.1029/2002JA009389.

Tsyganenko, N. A. (1995), Modelling the Earth's magnetospheric magnetic field confined within a realistic magnetopause, *J. Geophys. Res.*, *100*(A4), 5599–5612, doi:10.1029/94JA03193.

Vasyliunas, V. (1968), A survey of low-energy electrons in the evening sector of the magnetosphere with OGO 1 and OGO 3, *J. Geophys. Res.*, *73*(9), 2839–2884.

Waters, C. L., B. J. Anderson, and K. Liou (2001), Estimation of global field aligned currents using the Iridium® system magnetometer data, *Geophys. Res. Lett.*, *28*(11), 2165–2168, doi:10.1029/2000GL012725.

Yao, Z. H., et al. (2012), Mechanism of substorm current wedge formation: THEMIS observations, *Geophys. Res. Lett.*, *39*, L13102, doi:10.1029/2012GL052055.

Zheng, Y., K. A. Lynch, M. Boehm, R. Goldstein, H. Javadi, P. Schuck, R. L. Arnoldy, and P. M. Kintner (2003), Multipoint measurements of field-aligned current density in the auroral zone, *J. Geophys. Res.*, *108*(A5, 1217), doi:10.1029/2002JA009450.